ACS APPLIED NANO MATERIALS

Subscriber access provided by Kaohsiung Medical University

Article

Unconventional Shape Memory Mechanisms of Nanoporous Polymer Photonic Crystals: Implications for Nanooptical Coatings and Devices

Yongliang Ni, Yifan Zhang, Sin-Yen Leo, Yin Fang, Mingzhen Zhao, Long Yu, Kyle D. Schulze, Wallace Gregory Sawyer, Thomas E. Angelini, Peng Jiang, and Curtis Taylor

ACS Appl. Nano Mater., **Just Accepted Manuscript** • DOI: 10.1021/acsanm.8b01105 • Publication Date (Web): 17 Oct 2018

Downloaded from http://pubs.acs.org on October 21, 2018

Just Accepted

"Just Accepted" manuscripts have been peer-reviewed and accepted for publication. They are posted online prior to technical editing, formatting for publication and author proofing. The American Chemical Society provides "Just Accepted" as a service to the research community to expedite the dissemination of scientific material as soon as possible after acceptance. "Just Accepted" manuscripts appear in full in PDF format accompanied by an HTML abstract. "Just Accepted" manuscripts have been fully peer reviewed, but should not be considered the official version of record. They are citable by the Digital Object Identifier (DOI®). "Just Accepted" is an optional service offered to authors. Therefore, the "Just Accepted" Web site may not include all articles that will be published in the journal. After a manuscript is technically edited and formatted, it will be removed from the "Just Accepted" Web site and published as an ASAP article. Note that technical editing may introduce minor changes to the manuscript text and/or graphics which could affect content, and all legal disclaimers and ethical guidelines that apply to the journal pertain. ACS cannot be held responsible for errors or consequences arising from the use of information contained in these "Just Accepted" manuscripts.

ACS Publications

is published by the American Chemical Society. 1155 Sixteenth Street N.W., Washington, DC 20036

Published by American Chemical Society. Copyright © American Chemical Society. However, no copyright claim is made to original U.S. Government works, or works produced by employees of any Commonwealth realm Crown government in the course of their duties.

Unconventional Shape Memory Mechanisms of Nanoporous Polymer Photonic Crystals: Implications for Nanooptical Coatings and Devices

Yongliang Ni,[†] Yifan Zhang,[†] Sin-Yen Leo,[‡] Yin Fang,[‡] Mingzhen Zhao,[§] Long Yu,[§] Kyle D. Schulze,[†] Wallace G. Sawyer,[†] Thomas E. Angelini,[†] Peng Jiang[‡], and Curtis R. Taylor*[†]*

[†]Department of Mechanical and Aerospace Engineering, University of Florida, Gainesville, Florida 32611,

[‡]Department of Chemical Engineering, University of Florida, Gainesville, Florida 32611,

[§]Department of Materials Science and Engineering, University of Florida, Gainesville, Florida 32611

KEYWORDS: shape memory polymers, photonic crystals, "cold" programming, Laplace pressure, physical competing relationship, semi-deformed stable state

Abstract

Shape memory photonic crystals may hold the key to the continuing development of smart optical coatings and next-generation all-optical integrated circuits. The reconfigurability of these materials in response to various external stimuli is not only aesthetically appealing but fundamentally important in guiding the design of emerging reconfigurable nanophotonic devices. Here we report a new type of polymer shape memory photonic crystal (PSMPC) that shows autonomous Laplace pressure-driven, elastic modulus-dependent microstructural programming and solvent-swelling-triggered shape memory recovery, all occur at room temperature. By varying the compositions of their constituent polymers, the elastic moduli of the PSMPCs can be systematically modulated, leading to different photonic bandgaps (i.e., diffractive colors) in response to different solvents, such as water, ethanol, and acetonitrile. The different diffractive colors represent varied strains stored in the semi-deformed nanoporous PSMPCs. A new physical competing relationship, denoted by a dimensionless parameter, μ, between the elastic modulus of polymer and the surface tension of solvent, was established to characterize the range within which the nanoporous photonic crystal structure can stay in the semi-deformed stable state upon the application of solvents with different surface tensions. Good overlapping in the range of μ was observed from PSMPCs deformed by water, ethanol, and acetonitrile, which verified the applicability of this competing relationship in predicting the "cold" programming behaviors of the nanoporous PSMPCs. This fundamental study will pave the way for the rational design of nanoporous PSMPCs with optimized mechanochromic properties that can be used in a broad spectrum of tunable nanooptical applications.

1. Introduction

Since the concept of photonic crystal was first proposed in 1987, they have sparked enormous interest because of their tremendous potentials for controlling the flow of light in miniature volume.[1,2,11–13,3–10] This capability in manipulating photons (light) can ultimately lead to all-optical integrated circuits and high-speed optical computing.[12,14] By incorporating microstructural reconfigurability into traditional passive photonic crystals using various stimuli-responsive materials, active/adaptive photonic materials and devices have been developed.[14-33] Unfortunately, for most of the currently available tunable photonic crystals, they will quickly return to their original configurations once the external stimuli are removed. Although this rapid microstructural reversibility is ideal for some applications (e.g., displays), it impedes many others that require fixed intermediate structures, such as truly rewritable/reconfigurable nanooptics, mode-locked filters and lasers, mechanochromic impact sensors, and photonic random access memories.[12,14,21]

Recently, the discovery of nanoporous PSMPCs by Yin *et al.* overcame the drawback of transient intermediate states and provides a promising pathway to the further development of truly reconfigurable photonic crystals towards real-world applications. By integrating proper shape memory polymers (SMPs) with unique three-dimensionally (3-D) ordered nanoporous microstructures, PSMPCs with reconfigurable/rewritable properties have been demonstrated.[25,34–37] These PSMPCs can be programmed (transition from a permanent shape to a temporary one) by controlling the evaporation of water (for hydrophilic SMPs) or various swelling solvents (for hydrophobic polymers) in the interconnecting nanopores, and then recovered back to their permanent shapes in response to a spectrum of external stimuli, such as heat, multiple solvents and vapors, and various mechanical stresses (e.g., static pressure, lateral

shear stress, and ballistic impact). In addition to enabling striking structural colors, the unique nanoporous inverse opal structure of PSMPCs is critical in achieving the nontraditional evaporation-induced SM programming. Furthermore, unlike traditional thermoresponsive SMPs that require heat in programming and recovery processes during the shape memory cycle, these PSMPCs can be "cold" programmed, stored, and recovered all at room temperature. This nontraditional all-room-temperature SM effect could significantly expand the material processability and selection for many important technological applications such as biometric recognition,[25] chemical sensing,[34,36] and reconfigurable micropatterning.[37]

The unusual "cold" programming mechanism of the PSMPCs triggered by solvent evaporation was attributed to surface tension-induced microstructural deformation,[25] which belongs to the generic type of athermal solvent-activated programming.[38–47] The shape memory recovery triggered by various solvents with low surface tensions (e.g., acetone and ethanol) could be explained by the entropy elasticity of the polymer chains[48–56] that was activated by solvent-induced plasticizing effects.[38,39,46–48] However, the panorama of the underlying shape memory mechanisms in these PSMPCs with unique nanoporous photonic crystal microstructures are still far from being well-understood. Specifically, the underlying mechanisms regarding how the deformed nanopores are fixed after "cold" programming and what parameters govern the deformation behavior of these PSMPCs remain unanswered. Systematic fundamental studies on the material and physical properties (e.g., polymer elasticity and solvent surface tension) that govern this unconventional all-room-temperature shape memory effect (SME) are thus critical in achieving rational designs of new reconfigurable nanooptical materials and devices.

Herein we report the systematic experimental and theoretical investigations on a new series of nanoporous PSMPCs with varying polymer compositions that show predictable polymer

elasticity-dependent deformation behaviors upon the application of solvents with different surface tensions. In sharp contrast to one completely deformed temporary state as reported in our previous work, this new series of PSMPCs exhibit multiple semi-deformed stable states when dried out of solvents with different surface tensions. By thoroughly characterizing the competing contributions of varying the elastic modulus of polymer and surface tension of applied solvent on the deformation behavior of these PSMPCs, this study provides better understanding of the basic shape memory mechanisms in this new series of smart material. A new governing physical competing relationship between the elasticity of polymer and the surface tension of solvent is proposed and evaluated to verify that the "cold" programming of nanoporous PSMPCs can be tuned through changing the elasticity of polymer (i.e., polymer composition). The results of this study are useful in guiding the material selection and process optimization of nanoporous PSMPCs in emerging applications such as thin-film smart optical coatings and reconfigurable nanophotonic circuits.[9,11,62–67,13,15,20,57–61]

2. Experimental Section

2.1. Preparation of Nanoporous PSMPCs. Two commercial photocurable oligomers, polyethylene glycol diacrylate (PEGDA) (SR 259, molecular weight ~ 200 g/mol, and refractive index ~ 1.464) and polyethylene glycol dimethacrylate (PEGDMA) (SR 740, molecular weight ~ 1000 g/mol, and refractive index ~ 1.460), were obtained from Sartomer. They were mixed in different weight ratios from 67% to 10% of PEGDA content for 5 min using a vortex mixer. Darocur 1173 (2-hydrooxy-2-methyl-1-phenyl-1-propanone, BASF, 1 wt.%) was added as photoinitiator. Nanoporous PSMPCs were fabricated via the following steps. First, silica microspheres with nominal diameter of ~ 290 nm obtained from Particle Solutions LLC (Alachua, FL) were self-assembled on a clean glass microslide via the convective self-assembly

method.[68] Next, the colloidal crystals grown on both sides of the glass microslide were sandwiched by two other glass substrates, followed by infiltrating the pre-mixed oligomer mixture into the sandwich structure and photocuring the oligomers using 365 nm UV light generated by a UV transilluminator (UV95041401 from Fisher) for 90 min. The silica microspheres were removed from the polymer matrix by etching in a 2 vol.% hydrofluoric acid aqueous solution for 2 hours. The samples were finally rinsed with deionized water and dried in air to obtain self-standing nanoporous SMP membranes. The resulting samples were about 3 × 1.5 × 0.1 cm^3 (length × width × thickness).

2.2. Sample Characterization. Differential scanning calorimetry (DSC) thermograms were obtained using a Q1000 unit from TA Instruments at a heating rate of 10 °C min^{-1} and an empty pan as reference. The photonic bandgaps (PBGs) of the PSMPCs were characterized by using an Ocean Optics HR4000 high-resolution fiber optic visible-near infrared spectrometer with a tungsten halogen light source (LS-1). Absolute reflectivity was obtained as the ratio of the sample spectrum and a reference spectrum, which was collected using an aluminum-sputtered (~ 1 μm thickness) silicon wafer. The scanning electron microscope (SEM) images of the PSMPC samples in their deformed and recovered states were obtained with a FEI XL-40 FEG SEM. A thin layer of Au (~ 5 nm) was coated onto sample surfaces prior to imaging. Atomic force microscope (AFM) was used in obtaining the surface topographies of PSMPCs. The amplitude-modulation scan mode was performed using a MFP-3D AFM (Asylum Research, Inc.) and a Nanosensor PPP-NCHR probe (tip radius < 10 nm). Surface topographic images with 3 × 3 μm^2 size (256 × 256, pixels × lines) were scanned for each PSMPC composition. The pixel resolution of images is ~ 12 nm. The AFM images were post-processed by Scanning Probe Imaging Processor software for 3-D rendering, roughness calculation, etc. Micro-indentation was

performed on dry nanoporous PSMPCs (dried in air for more than 48 hours) using a Hysitron BioSoft™ In-situ Indenter. The instrument is equipped with a three-plate conductive transducer[69] of nano-Newton force resolution and a *Z*-piezo capable of 150 μm depth indentation. The system was calibrated by an air indent step to measure the voltage-distance constant. Samples were mounted on a specialized clamp with a transparent glass substrate. A sapphire spherical indenter tip with 1.6 mm radius was used in every measurement. The experiments were performed with a displacement-controlled indentation (0.5 and 5 μm maximum depth) at a constant rate of 0.1 μm/s. Three areas per sample and two samples per copolymer composition were tested for all PSMPCs. All measurements were performed at room temperature and relative humidity of 40-50%. For calculation of the effective elastic modulus, the Johnson-Kendall-Roberts (JKR) model[70] of elastic contact was fitted to the unloading portion of the indentation curve.

3. Results and Discussion

3.1. Preparation and Characterization of Nanoporous PSMPCs with Varying Compositions. Two water soluble functional oligomers, PEGDA and PEGDMA with molecular structures shown in Figure S1 (Supporting Information), were mixed in different weight ratios (from 67% to 10% of PEGDA content) prior to preparing nanoporous PSMPCs by using convectively self-assembled silica colloidal crystals comprising ~ 290 nm diameter silica microspheres as structural templates.[68,71,72] The schematic illustration in Figure 1a shows the basic operating principles of the templated nanoporous PSMPCs. When dried out of a solvent with a high surface tension (e.g., water), the periodic nanopores are collapsed. By contrast, when dried out of a solvent with a low surface tension (e.g., ethanol), the collapsed nanopores can be recovered. The glass transition temperatures of pure PEGDA and PEGDMA polymers, as well as their copolymers with different compositions, were characterized by differential scanning

calorimetry and the results are shown in Figure S2 and Table S1 in the Supporting Information. PEGDA has a higher T_g (~ -5 °C) and a broader glass transition (from ~ -57 °C to ~ 47 °C) than those of PEGDMA (~ -53 °C and from ~ -57°C to ~ -49°C). The effective elastic moduli of the resulting PSMPC membranes with different copolymer compositions, which can be tuned in the range between the elastic moduli of the two oligomers, were characterized by *in-situ* micro-indentation tests. The experimental indentation curves (see Figure S3 in the Supporting Information) were fitted by using the JKR contact mechanics model considering a large pull-off force (adhesion) observed in detachment to calculate the copolymer effective elastic moduli. The final micro-indentation results are summarized in Figure 1b. Apparently, pure PEGDA polymer has a much higher effective elastic modulus (~ 100 MPa) than that of PEGDMA (< 0.3 MPa). By increasing the content of PEGDA in the final copolymers, their effective elastic moduli increase. This result is quite reasonable considering the different molecular weights of PEGDA and PEGDMA oligomers. Higher content of much longer PEGDMA oligomers in the shape memory copolymers can lead to lower cross-linking density and larger mesh size, thus resulting in smaller effective elastic modulus and higher deformability.

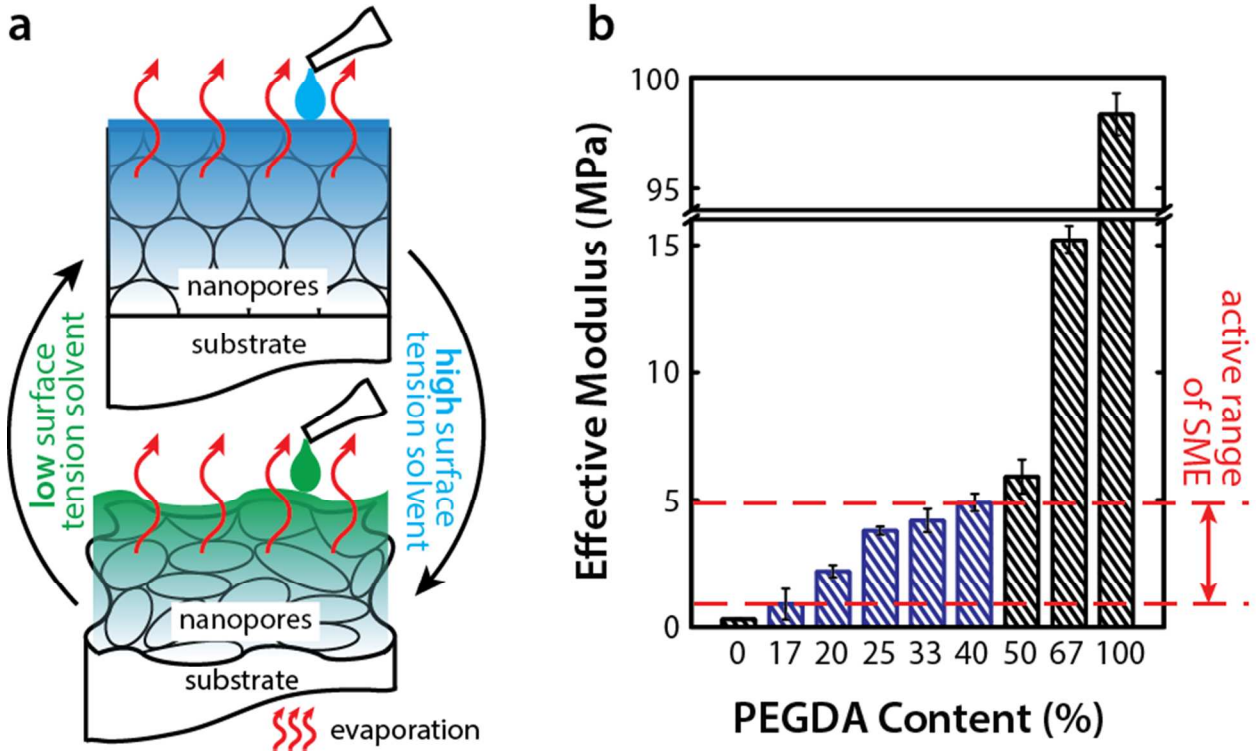

Figure 1. (a) Schematic illustration of solvent-evaporation-induced shape memory cycle of nanoporous PSMPC. (b) Effective elastic moduli of PSMPCs with varying copolymer compositions.

3.2. Composition-dependent Deformation of Nanopores in PSMPCs. During the templating nanofabrication of PSMPC membranes, the silica microsphere scaffolds were removed by etching in a hydrofluoric acid aqueous solution, followed by thorough wash using deionized water. After dried out from water under compressed air for ~ 10 s, the PSMPC samples showed drastically different colors depending on their polymer compositions, as shown in the photographs and the normal-incidence optical reflection spectra in Figure 2a and 2b. The sample comprising 67% PEGDA exhibited shining greenish diffractive color and its reflection spectrum matched well with that of the nanoporous photonic crystal with un-deformed nanopores prepared using the same batch of colloidal crystal templates and pure PEGDA oligomer. As the

refractive index of PEGDA is nearly the same as that of PEGDMA, the overlap of the optical reflection spectra indicates the dried PSMPC membrane with 67% PEGDA maintained its permanent photonic crystal structure with un-deformed nanopores. By contrast, the PSMPC samples with lower PEGDA contents (from 60% to 40%) showed different diffractive colors and apparent blue shifts in the positions of the corresponding PBGs (from ~ 515 to ~ 480 nm). These drastic color changes indicated that the permanent periodic configurations of the templated nanoporous photonic crystals were gradually changed to multiple structurally "fixed" temporary states as their structural colors were mainly determined by the lattice spacing of the semi-deformed photonic crystals. Interestingly, the PSMPC samples containing < 40% PEGDA became nearly transparent after dried out from water and no distinctive PBGs were present in their reflection spectra. In addition, the maximum optical reflection amplitudes of the PBGs shown in Figure 2c, which are good indicators of the crystalline order of the PSMPCs, significantly decreased for samples with < 40% PEGDA. By simultaneously considering the above optical and mechanical properties of the PSMPC samples with different copolymer compositions, it is clear that PEGDA-co-PEGDMA copolymers with decreasing effective elastic moduli (i.e., decreasing PEGDA content) experienced larger microstructural deformation during water evaporation from the nanopores.

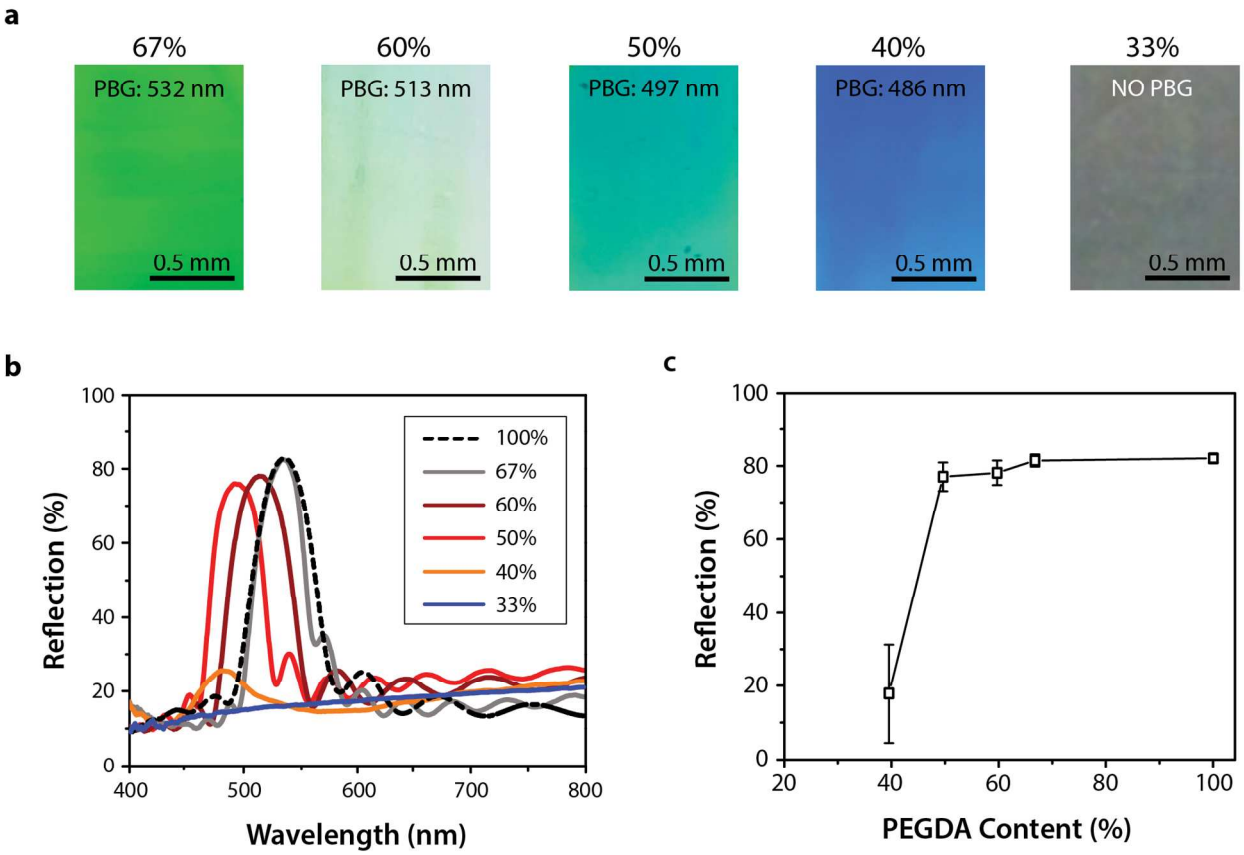

Figure 2. PSMPC membranes with different copolymer compositions showing drastically different diffractive colors after dried out from water. a) Photographs and PBG peak positions of the PSMPCs containing 67%, 60%, 50%, and 40% PEGDA. b) Normal-incidence optical reflection spectra of the PSMPCs with different PEGDA contents. c) Maximum optical reflection amplitudes of the PBGs of the PSMPCs with different PEGDA contents.

Surprisingly, we found that the deformed nanopores triggered by water evaporation could be partially recovered when the PSMPC membranes with low PEGDA contents were dried out from ethanol under compressed air for ~ 5 s, leading to the reappearance of structural colors of these otherwise transparent samples. The photographs and normal-incidence optical reflection spectrum in Figure 3a and 3b showed that PSMPCs with the PEGDA content as low as 17% still exhibited distinct diffractive colors and PBGs after dried out from ethanol. Similarly, clear trends of blue shift in the PBGs (Figure 3b) and gradual decrease of the maximum reflection amplitudes

of PBGs (Figure 3c) were observed in the PSMPCs as the content of PEGDA decreased. However, the samples containing < 17% PEGDA became nearly transparent and showed no distinctive PBGs in the reflection spectra after ethanol evaporation.

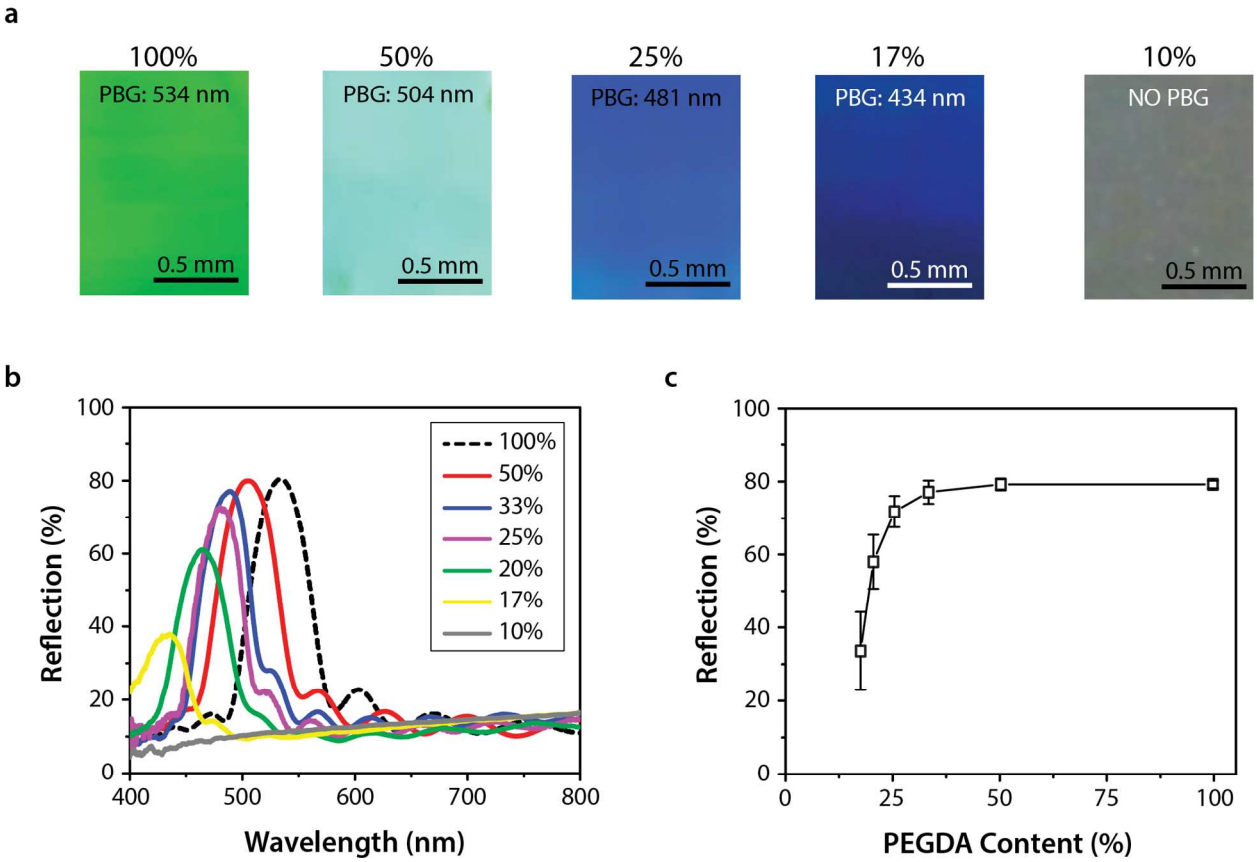

Figure 3. a) Photographs of PSMPCs with varied PEGDA contents showing different diffractive colors after dried out from ethanol. b) Normal-incidence optical reflection spectra of the PSMPCs with PEGDA contents ranging from 10% to 100%. c) Maximum optical reflection amplitudes of the PBGs of the PSMPCs with different PEGDA contents.

3.3. Active Range of Shape Memory Effect in PSMPCs. The SME of the PEGDA-co-PEGDMA PSMPCs is defined based on their structural deformation behaviors after dried out from water and ethanol. Choosing ethanol and water as two representative solvents is because they have very different surface tension: ~ 72 mN/m for water and ~ 21 mN/m for ethanol (both at 25 °C). If both the phenomena, that are, without reflecting PBGs after the application of water

and with reflecting PBGs after the application of ethanol, are observed in the PSMPCs with certain compositions, these PSMPCs are classified to be within the active range of SME. The all-room-temperature shape memory cycle of these PSMPCs can then be defined by two steps, which are water-evaporation-induced shape memory "cold" programming and ethanol-swelling-induced shape memory recovery. The temporary/intermediate structures correspond to the deformed nanopores caused by "cold" programming of PSMPCs exhibiting active SME.

The morphological changes of PSMPCs in the shape memory cycle were characterized using cross-sectional SEM imaging. Initially, the highly ordered nanoporous structure consisting of 67% PEGDA and nominal 290 nm diameter nanopores is shown in the SEM image in Figure 4a. After the water-evaporation-induced "cold" programming step, PSMPCs within the active range of SME immediately lost their original diffractive colors as shown by the photo in Figure 4e. From the SEM images of the PSMPC after water evaporation (Figure 4d and 4f), a disordered nanoporous structure with morphing of pores and an undulating surface was observed. This indicates that the loss of the diffractive color originates from the nanopore deformation and the destruction of structural periodicity. After the application of ethanol, the reflecting color was regained for PSMPCs with certain compositions. The photos and SEM image of the recovered PSMPCs demonstrate that the deformed nanoporous structures partially return to their original, periodic configuration as shown in Figure 4b and 4c. It is worthy to mention that this programming-recovery cycle can be easily realized by drying the templated PSMPCs consecutively out of water ("cold" programming) and ethanol (recovery).

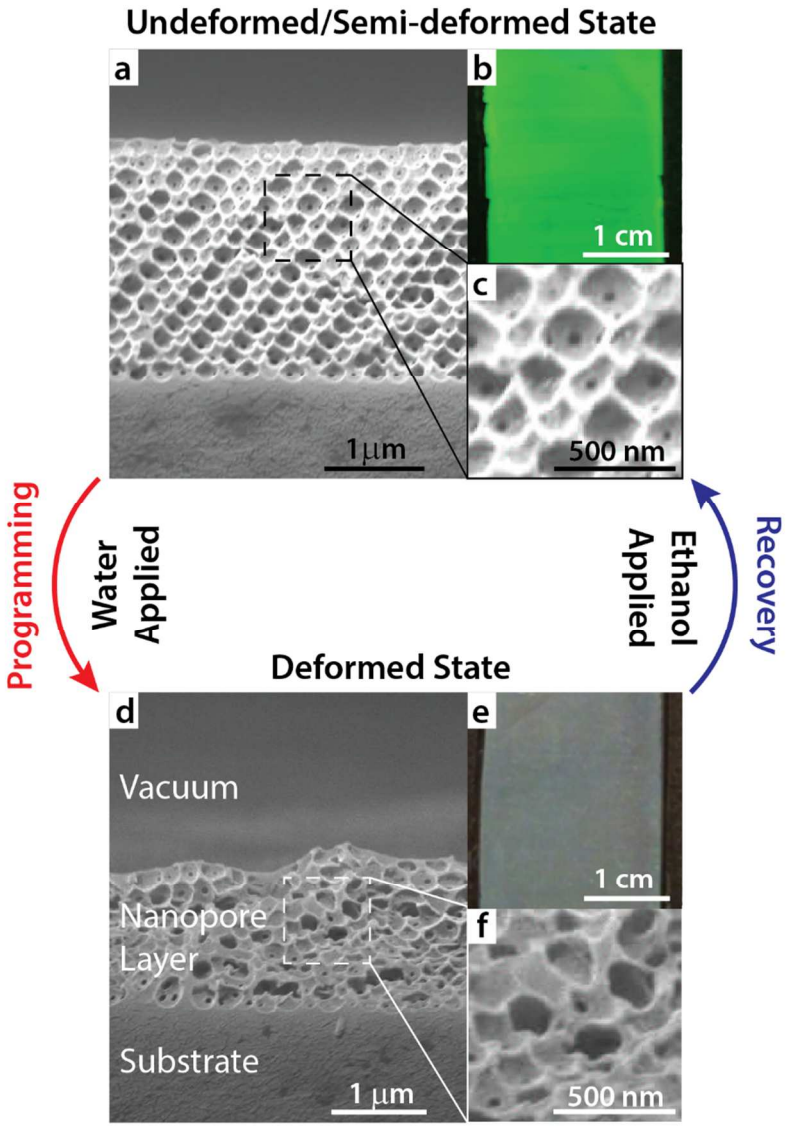

Figure 4. All-room-temperature shape memory cycle of nanoporous PSMPCs consisting of 67% PEGDA. Cross-sectional SEM images of the nanoporous photonic crystal structure in its a) undeformed/semi-deformed and d) completely deformed state. Insets b) and e) showing photographs of the corresponding PSMPC samples. Insets c) and f) showing the magnified morphologies of the nanoporous structures.

For PSMPCs comprising > 40% PEGDA, the evaporation of water was unable to completely deform the nanoporous structures (see Figure 2b); while for PSMPCs with < 17% PEGDA, ethanol was unable to recover the completely "cold"-programmed nanopores (see Figure 3b). Therefore, 40% and 17% of PEDGA contents set the upper and lower limits,

respectively, of the active range of SME for these two applied solvents. A schematic of the active range of SME in these PSMPCs, along with representative AFM images of the PSMPCs with different compositions, are shown in Figure 5.

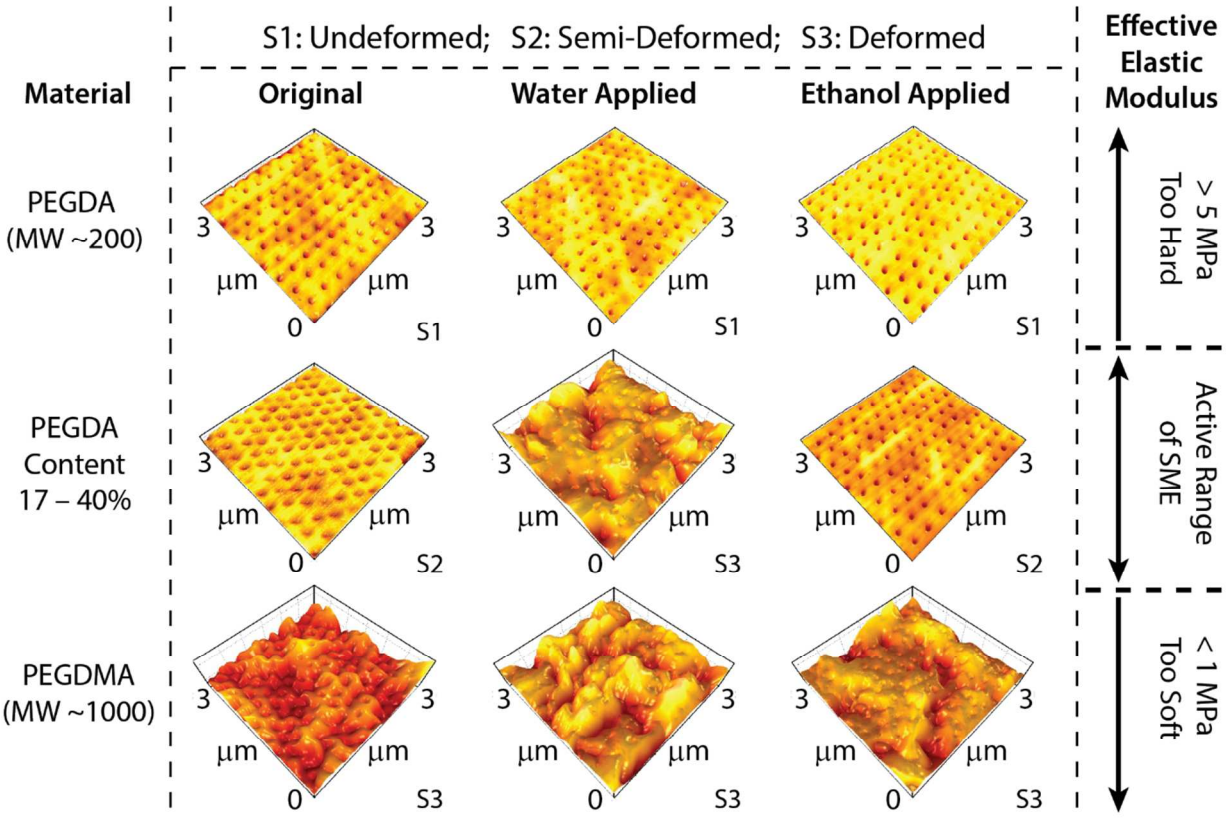

Figure 5. Representative AFM images of nanoporous PSMPC surfaces made from pure PEGDA, copolymers with 17-40% PEGDA, and pure PEGDMA in their original, water applied, and ethanol applied states. These images are used in identifying the active range of SME in the scale of effective elastic modulus.

3.4. Measuring Strains of PSMPCs Using Cross-sectional SEM and Optical Spectroscopy. Two different approaches were used in characterizing the stored strains in semi-deformed PSMPCs. The first straightforward approach was based on cross-sectional SEM imaging. The SEM images in Figure 6a compare PSMPC samples with different PEGDA contents after ethanol recovery. For the pure PEGDA sample (labeled as 100% in Figure 6a), the measured number of nanopore layers was $n = 13$ and the thickness of the original, undeformed

nanoporous photonic crystal layer was about 2814 ± 67 nm. This thickness was then used in calculating the residual compressive strains (defined as decrease in thickness/original thickness) stored in the semi-deformed PSMPCs with different PEGDA contents, which were labeled in the SEM images and summarized in Figure 6b. Higher strains were observed in PSMPCs with lower PEGDA contents (i.e., smaller effective elastic moduli).

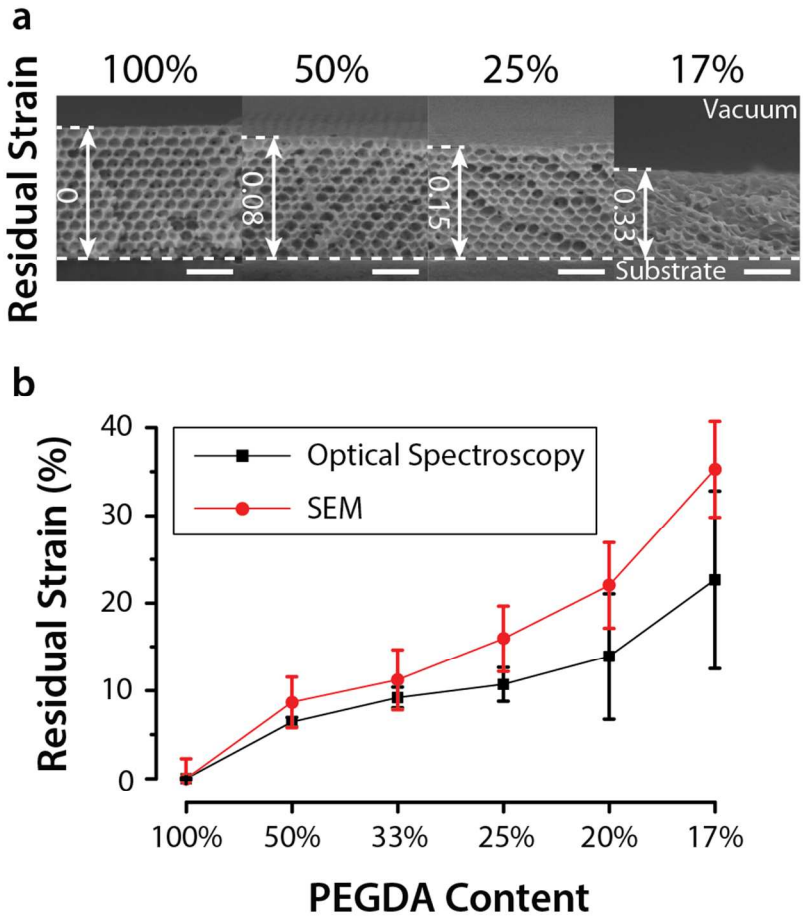

Figure 6. a) Cross-sectional SEM images of PSMPCs with different PEGDA contents after ethanol recovery. The scale bars in the figures stand for 1 μm. b) Comparison of residual strains of different PSMPCs measured by optical spectroscopy and cross-sectional SEM.

Complementing the time-consuming SEM characterization, the *in-situ*, noninvasive optical reflection measurement provides a much simpler and faster methodology in quantitatively evaluating the level of deformation (i.e., stored strains) in the nanopores. It is well-known that

the peak positions of the PBGs are sensitive to the change in lattice spacing of the nanoporous photonic crystals. The PBGs in the normal-incidence reflection spectra are caused by Bragg diffraction of incident light from the stacked (111) crystallographic planes of the templated PSMPCs possessing face-centered cubic (FCC) crystal structure. A blue shift of the PBG peak represents a decreasing lattice spacing hence a compression in the thickness direction of the nanoporous structure. The diffractive peak position of the nanoporous photonic crystal can be described according to Bragg's law of diffraction:[8]

$$\lambda = 2n_{eff}dsin\theta \quad (1)$$

$$n_{eff} = \phi n_{air} + (1-\phi)n_{polymer} \quad (2)$$

$$d = \frac{\sqrt{2}}{\sqrt{3}} D_{macropore} \quad (3)$$

where λ is the PBG wavelength, n_{eff} is the effective reflective index of the nanoporous PSMPC, d is the lattice spacing, $D_{macropore}$ is the diameter of the nanopores, ϕ is the volume fraction of air (~ 0.74 in this case), n_{air} and $n_{polymer}$ are refractive index of air and SMP, respectively, and θ is the light incident angle. By using this *in-situ* optical characterization technique, the calculated thickness of the undeformed PEGDA nanoporous photonic crystal was about 2840 nm, which is in good agreement with the value determined by SEM. Figure 6b summarizes the calculated strains (using the Bragg's law) of the nanoporous structure from the measured shifts in the PBG wavelengths (see Figure 3b).

After application of ethanol, the residual strains in the nanoporous structures of PSMPCs with varying PEGDA contents (from 17% to 50%) changed from ~ 21% to ~ 9%. These optically derived values are directly compared with the strains measured from the cross-sectional SEM images in Figure 6b. An increased difference between the measured strains by SEM imaging and

optical spectroscopy was observed in PSMPCs with larger deformations. This discrepancy can be attributed to the lack of considering the superposed increase in n_{eff} of nanoporous photonic crystals during the decrease in lattice spacing. An underestimation in the deformation of the nanoporous structure was thus introduced by this lack of consideration when constant n_{eff} was used in the calculations using the Bragg's law of diffraction.

3.5. Shape Memory Mechanisms of PSMPCs. In our previous work, we demonstrated that the "cold" programming triggered by water evaporation could be attributed to the dominancy of high water surface tension over the polymer elasticity. When solvent molecules are absorbed into the polymer network, they may induce the plasticizing effect that fully relaxes the physically entangled macromolecular chains,[73,74] increasing their mobility and reducing the polymer elastic modulus. During shape memory recovery, entropy elasticity drives the stretched polymer chains back to their original, energy favorable configurations upon the release of the fixed strain. However, the strain fixation mechanism has not been explained in our previous work, which will be specified in the following paragraphs.

There are two stages, i.e., deformation and fixation, which lead to the residual strain in the nanoporous structure of PSMPCs. During the process of water evaporation from the interconnecting nanopores, a water membrane will ultimately form that covers the surface of the nanopores. This water membrane will generate an inward Laplace pressure, which tends to collapse the nanoporous structure to minimize the exposed surface area of water. Due to the small interconnecting holes between the nanopores (see Figure 4c), all the nanopores in the PSMPC membrane are connected to the ambient air. Thus, each of the nanopores can be treated as an open inclusion with air inside, where no Laplace pressure can exist to support the nanoporous structure. Water surface tension, which has the equivalent magnitude as the Laplace

pressure used to balance it, acts as the driving force to deform the nanoporous structure. If water surface tension dominates over polymer elasticity, it will drive the collapse of the ordered nanopores. In the subsequent strain fixation stage, most of the water molecules have been evaporated from the hydrophilic polymer network. Secondary intermolecular forces (e.g., van der Waals interactions between the entangled polymer chains) will "freeze" the polymer network in their deformed conformations. Hence, some elastic energy will be stored in the deformed polymer chains. This strain fixation mechanism (acting as a molecular switch), combined with Laplace pressure-induced deformation in the nanoporous structure, enables the unique SME of PSMPCs.

3.6. Physical Competing Relationship: Polymer Elasticity vs. Laplace Pressure. A new physical competing relationship between the elasticity of polymer matrix and the surface tension of liquid was established to qualitatively describe the deformations and the corresponding optical properties of the nanoporous PSMPCs. We first considered the case of a closed air inclusion in liquid (see Figure 7a), where the surface tension of liquid tends to diminish its exposed surface area and is equilibrated by the boosted pressure in the inclusion. If a channel exists to connect the inside air to outside atmosphere, the surface tension of liquid will push out the air and drive the collapse of the inclusion. This open air inclusion in liquid is similar to the interconnected nanopores in PSMPCs (as shown in the scheme in Figure 7b), which are encapsulated by solvent-absorbed polymer matrix. The absorbed solvent on the nanopore walls will generate a surface tension at its exposed surface in the nanoporous structure that tends to collapse the nanopores. However, this tendency is resisted by the stiffness of the polymer matrix. From an energy perspective, this competing relationship can be described by the ratio of liquid surface energy ($E_{surface} = \gamma_l \cdot A_{diminished}$) and elastic restoring energy ($E_{restoring} = E_{polymer} \cdot$

$V_{deformed}$) that works against the nanopore collapse. The diminishing area is proportional to the surface area of a nanopore, i.e., $A_{diminishing} \propto 4\pi r_{macropore}^2$, and the deformed volume is proportional to the volume of a nanopore, i.e., $V_{deformed} \propto \frac{4}{3}\pi r_{macropore}^3$. The gravitational contribution to the deformation of the nanoporous structure (elastic modulus of MPa scale) is negligible. The resulting competing parameter, μ, can be written as:

$$\mu = \frac{E_{restoring}}{E_{surface}} = constant \cdot \frac{r_{macropore} E_{polymer}}{\gamma_l} \qquad (4)$$

where γ_l is the liquid surface tension, $E_{polymer}$ is the effective elastic modulus of the polymer matrix, $r_{macropore}$ is the radius of the nanopores of PSMPCs.

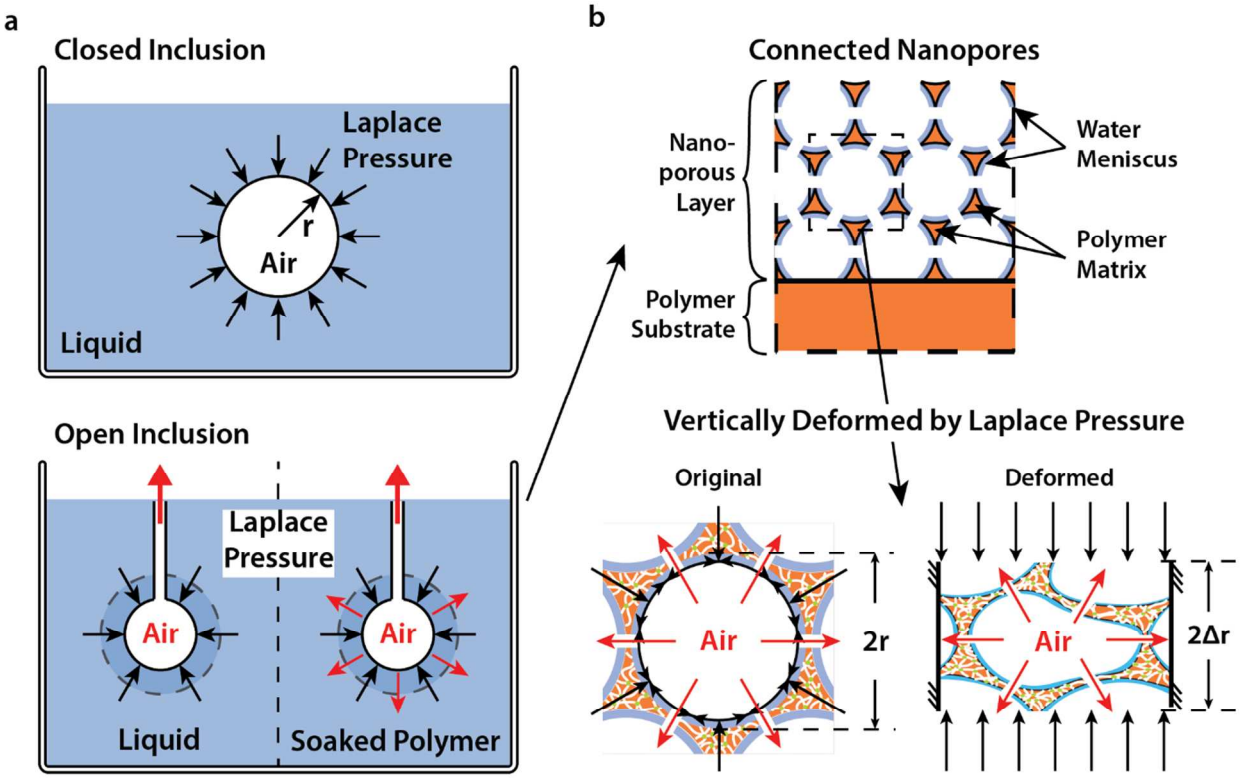

Figure 7. Schematic illustrations showing similar deformation mechanisms driven by Laplace pressures in a) closed inclusion in liquid and open air inclusions in both liquid and soaked polymer, and b) interconnecting nanoporous structure.

When $\mu \ll 1$, surface tension dominates and the PSMPC will always stay in a deformed, optically transparent state; while when $\mu \gg 1$, polymer elasticity dominates and the PSMPC will always remain in its ordered, iridescent state. When $\mu \sim 1$, the PSMPC will possess active tunability of reversible structural switching. One simplification to point out is that the deformation in the nanoporous structure can be treated as one-dimensional deformation in the thickness direction because the lateral deformation is constrained by the thick and solid polymer base layer, which is nearly three orders of magnitude thicker than the nanoporous layer and provides the mechanical stability to the micrometer-thick nanoporous structure. This simplification is compatible with both the observed elliptical nanopore morphology in SEM images (see Figure 6a) and the calculations of the residual strains using thickness-dependent PBG shifts in optical reflection spectra of the semi-deformed PSMPCs.

3.7. Using Competing Parameter μ to Characterize Active Ranges of PSMPCs by Various Solvents. To verify the feasibility of using the new competing parameter μ in characterizing the SME of PSMPCs, we compared the range of μ where semi-deformed temporary states can exist in the deformed PSMPCs induced by evaporation of three different solvents, i.e., water, ethanol, and acetonitrile. It is reasonable to speculate that the polymer network and thus the nanoporous structure of PSMPCs can be recovered back to the original, undeformed state caused by polymer swelling induced by adsorbed solvent.[75,76] This shape memory recovery can be easily characterized by the reappearance of the Bragg diffraction peaks, when the PSMPC samples were submerged in various solvents. However, the different phenomena observed after the application of water and ethanol, namely SM programming and recovery, respectively, are due to the surface tension difference between the two solvents. In a PSMPC sample of certain elastic modulus, ethanol with a smaller surface tension (~ 21 mN/m at

25 °C, less than one third of water surface tension of ~ 72 mN/m) should induce less deformation in the nanoporous structure than that caused by water. This explains why ethanol can be used in partially recovering the water-deformed nanopores. Similarly, hexane with an even smaller surface tension (~ 18 mN/m) can further red-shift the PBG wavelength of an ethanol applied PSMPC comprising 33% PEGDA (see Figure S4 in the Supporting Information), indicating a more complete recovery of the "cold" programmed nanopores. However, the optical spectra also show that the stored strains in PSMPCs with semi-deformed stable states cannot be erased completely by using solvents with low surface tensions.

Acetonitrile with a surface tension of ~ 29 mN/m at 25 °C was also applied to the PSMPCs with PEGDA contents ranging from 17% to 50% to further verify the new physical competing relationship. The resulting strains induced by acetonitrile, together with the ones triggered by ethanol and water evaporation, were plotted against the dimensionless competing parameter, μ, as shown in Figure 8. From the plot, we recognized that the surface tension-elasticity competing relationship could be used in predicting the active range where semi-deformed stable states can exist in PSMPCs. The upper-left region in Figure 8 represents that less strain will be stored at higher polymer elasticity. There is a threshold at $\mu \sim 3.5$ above which no residual strain induced by surface tension can be observed. The lower-right region on the other hand represents more strain will be induced at lower polymer elasticity. No elastic recovery can be observed below a threshold of $\mu \sim 0.3$. However, there is a difference in the residual compressive strains triggered by the evaporation of water, ethanol, and acetonitrile. This could be due to the different interfacial tensions acting between the solvent and polymer, as well as the different evaporation kinetics of the solvents.[77–80]

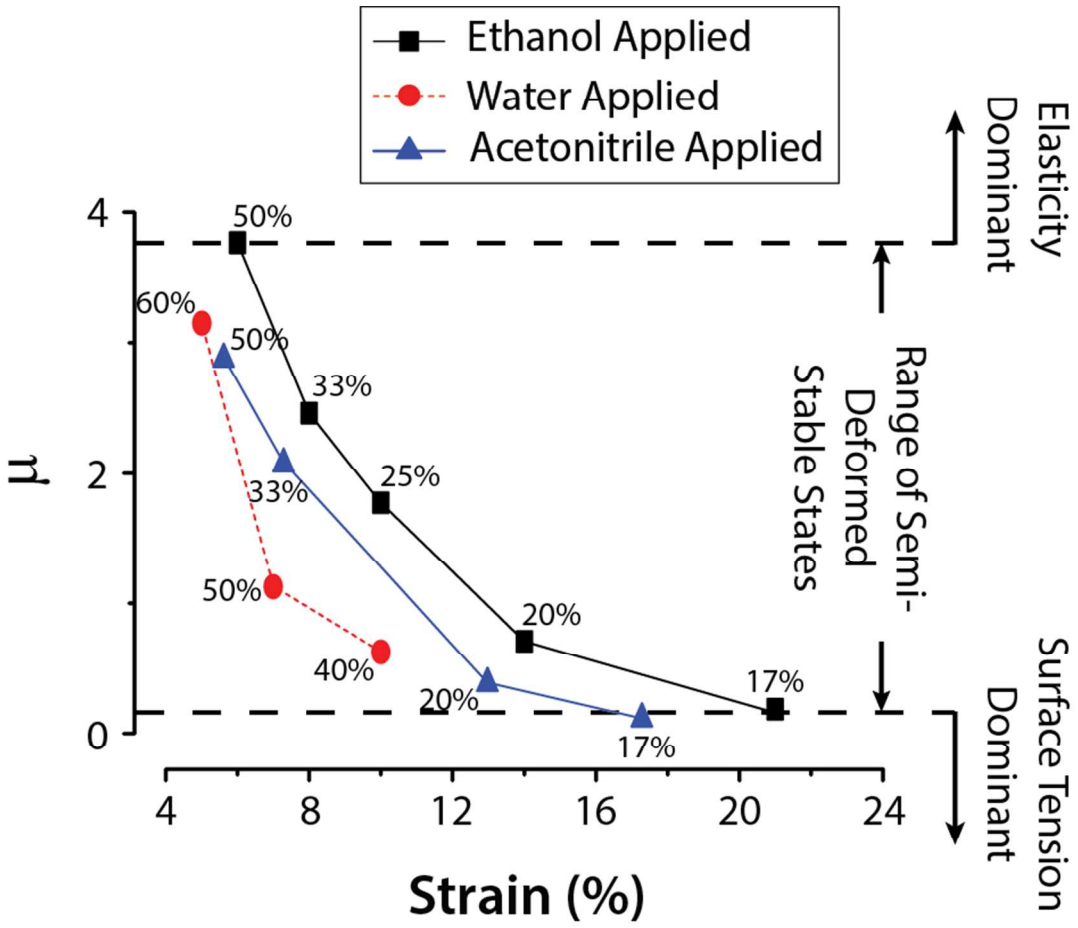

Figure 8. Plot of the active range of the dimensionless competing parameter, μ, within which semi-deformed stable states exist for various solvents (i.e., water, ethanol, and acetonitrile) with different surface tensions.

4. Conclusions

In conclusion, nanoporous PSMPC membranes of varying PEDGA-co-PEGDMA compositions were used in studying solvent-evaporation-induced, elastic modulus-dependent shape memory microstructural transformations. The different deformation behaviors observed in these PSMPCs upon the application of water and ethanol can be used in defining an active range of shape memory effect. A new physical competing relationship between the polymer elastic modulus and the surface tension of applied solvent was introduced to characterize the unique deformation behaviors in these PSMPCs, which provided better insights in understanding their

nontraditional, all-room-temperature shape memory mechanisms. Through the comparison of the dimensionless competing parameter, μ, in the cases of water, ethanol, and acetonitrile, an overlapping range where semi-deformed stable states in PSMPCs can exist is observed, which verifies the feasibility of using this competing relationship in predicting the autonomous deformation of PSMPCs. The results of this work can be used as guidelines for rational design of PSMPCs for next-generation reconfigurable nanooptical devices.

ASSOCIATED CONTENT

Supporting Information

Molecular structures of PEGDA and PEGDMA. Typical DSC plots of pure PEGDA and PEGDMA polymers and their copolymers with different compositions. Typical indentation force-displacement curves and JKR model fitting for calculating effective elastic moduli of various PEGDA-co-PEGDMA copolymers. Normal-incidence optical reflection spectra obtained from a pure PEGDA PSMPC and a PSMPC comprising 33% PEGDA dried out from hexane, ethanol, and water.

AUTHOR INFORMATION

Corresponding Author

*Curtis R Taylor, E-mail: curtis.taylor@ufl.edu.

*Peng Jiang, E-mail: pjiang@che.ufl.edu.

Author Contributions

Y.L.N., Y.F.Z., G.W.S, T.E.A., C.T., and P.J. conceived the research, established the model, and designed the experiments. Y.L.N., Y.F.Z., S.Y.L., Y.F., M.Z.Z., and L.Y. fabricated nanoporous PSMPC membranes and tested their optical, microstructural, and mechanical properties. Y.L.N.

Y.F.Z., and K.D.S. performed the AFM and indentation experiments. Y.L.N., C.T. and P.J. analyzed the data and wrote the manuscript. All authors reviewed and approved the manuscript.

ACKNOWLEDGMENT

This work was partially supported by the US Defense Threat Reduction Agency, Basic Research Award # HDTRA1-15-1-0022, to University of Florida. Acknowledgments were also made to the US National Science Foundation (NSF) under Award No. CMMI-1562861.

References

(1) Joannopoulos, J. J. D.; Johnson, S.; Winn, J. N. J.; Meade, R. R. D. *Photonic Crystals: Molding the Flow of Light*; 2008.

(2) Joannopoulos J.D, Pierre R. Villeneuve, S. F. Photonic Crystals:Putting a New Twist on Light. *Nature* **1997**, *386*, 143-149.

(3) Fudouzi, H.; Xia, Y. Colloidal Crystals with Tunable Colors and Their Use as Photonic Papers. *Langmuir* **2003**, *19*, 9653–9660.

(4) Valkama, S.; Kosonen, H.; Ruokolainen, J.; Haatainen, T.; Torkkeli, M.; Serimaa, R.; ten Brinke, G.; Ikkala, O. Self-Assembled Polymeric Solid Films with Temperature-Induced Large and Reversible Photonic-Bandgap Switching. *Nat. Mater.* **2004**, *3*, 872–876.

(5) Arsenault, A. C.; Clark, T. J.; von Freymann, G.; Cademartiri, L.; Sapienza, R.; Bertolotti, J.; Vekris, E.; Wong, S.; Kitaev, V.; Manners, I.; Wang, R. Z.; John, S.; Wiersma, D.; Ozin, G. A. From Colour Fingerprinting to the Control of Photoluminescence in Elastic Photonic Crystals. *Nat. Mater.* **2006**, *5*, 179–184.

(6) Potyrailo, R. A.; Ghiradella, H.; Vertiatchikh, A.; Dovidenko, K.; Cournoyer, J. R.; Olson, E. Morpho Butterfly Wing Scales Demonstrate Highly Selective Vapour Response. *Nat. Photonics* **2007**, *1*, 123–128.

(7) Xi, J.-Q.; Schubert, M. F.; Kim, J. K.; Schubert, E. F.; Chen, M.; Lin, S.-Y.; Liu, W.; Smart, J. A. Optical Thin-Film Materials with Low Refractive Index for Broadband Elimination of Fresnel Reflection. *Nat. Photonics* **2007**, *1*, 176–179.

(8) Aguirre, C. I.; Reguera, E.; Stein, A. Tunable Colors in Opals and Inverse Opal Photonic Crystals. *Adv. Funct. Mater.* **2010**, *20*, 2565–2578.

(9) Moon, J. H.; Yang, S. Chemical Aspects of Three-Dimensional Photonic Crystals. *Chem.*

Rev. **2010**, *110*, 547–574.

(10) Chattopadhyay, S.; Huang, Y. F.; Jen, Y. J.; Ganguly, A.; Chen, K. H.; Chen, L. C. Anti-Reflecting and Photonic Nanostructures. *Mater. Sci. Eng. R* **2010**, *69*, 1–35.

(11) Fenzl, C.; Hirsch, T.; Wolfbeis, O. S. Photonic Crystals for Chemical Sensing and Biosensing. *Angew. Chem. Int. Ed.* **2014**, *53*, 3318–3335.

(12) Chai, Z.; Hu, X.; Wang, F.; Niu, X.; Xie, J.; Gong, Q. Ultrafast All-Optical Switching. *Adv. Opt. Mater.* **2017**, *5*, 1600665.

(13) Fu, Q.; Zhu, B.; Ge, J. Hierarchically Structured Photonic Crystals for Integrated Chemical Separation and Colorimetric Detection. *Nanoscale* **2017**, *9*, 2457–2463.

(14) Grillet, C.; Monat, C.; Smith, C. L.; Lee, M. W.; Tomljenovic-Hanic, S.; Karnutsch, C.; Eggleton, B. J. Reconfigurable Photonic Crystal Circuits. *Laser Photonics Rev.* **2010**, *4*, 192–204.

(15) Ge, J.; Yin, Y. Responsive Photonic Crystals. *Angew. Chem. Int. Ed.* **2011**, *50*, 1492–1522.

(16) Kang, Y.; Walish, J. J.; Gorishnyy, T.; Thomas, E. L. Broad-Wavelength-Range Chemically Tunable Block-Copolymer Photonic Gels. *Nat. Mater.* **2007**, *6*, 957–960.

(17) Bedoya, A. C.; Domachuk, P.; Grillet, C.; Monat, C.; Magi, E. C.; Li, E.; Eggleton, B. J. Reconfigurable Photonic Crystal Waveguides Created by Selective Liquid Infiltration. *Opt. Express* **2012**, *20*, 11046–11056.

(18) Yue, Y. F.; Haque, M. A.; Kurokawa, T.; Nakajima, T.; Gong, J. P. Lamellar Hydrogels with High Toughness and Ternary Tunable Photonic Stop-Band. *Adv. Mater.* **2013**, *25*, 3106–3110.

(19) Schäfer, C. G.; Gallei, M.; Zahn, J. T.; Engelhardt, J.; Hellmann, G. P.; Rehahn, M.

Reversible Light-, Thermo-, and Mechano-Responsive Elastomeric Polymer Opal Films. *Chem. Mater.* **2013**, *25*, 2309–2318.

(20) Xu, H.; Yu, C.; Wang, S.; Malyarchuk, V.; Xie, T.; Rogers, J. A. Deformable, Programmable, and Shape-Memorizing Micro-Optics. *Adv. Funct. Mater.* **2013**, *23*, 3299–3306.

(21) Yang, D.; Ye, S.; Ge, J. From Metastable Colloidal Crystalline Arrays to Fast Responsive Mechanochromic Photonic Gels: An Organic Gel for Deformation-Based Display Panels. *Adv. Funct. Mater.* **2014**, *24*, 3197–3205.

(22) Sch??fer, C. G.; Lederle, C.; Zentel, K.; St??hn, B.; Gallei, M. Utilizing Stretch-Tunable Thermochromic Elastomeric Opal Films as Novel Reversible Switchable Photonic Materials. *Macromol. Rapid Commun.* **2014**, *35*, 1852–1860.

(23) Yang, D.; Qin, Y.; Ye, S.; Ge, J. Polymerization-Induced Colloidal Assembly and Photonic Crystal Multilayer for Coding and Decoding. *Adv. Funct. Mater.* **2014**, *24*, 817–825.

(24) Espinha, A.; Serrano, M. C.; Blanco, Á.; López, C. Thermoresponsive Shape-Memory Photonic Nanostructures. *Adv. Opt. Mater.* **2014**, *2*, 516–521.

(25) Fang, Y.; Ni, Y.; Leo, S.-Y.; Taylor, C.; Basile, V.; Jiang, P. Reconfigurable Photonic Crystals Enabled by Pressure-Responsive Shape-Memory Polymers. *Nat. Commun.* **2015**, *6*, 7416.

(26) Tippets, C. A.; Li, Q.; Fu, Y.; Donev, E. U.; Zhou, J.; Turner, S. A.; Jackson, A. M. S.; Ashby, V. S.; Sheiko, S. S.; Lopez, R. Dynamic Optical Gratings Accessed by Reversible Shape Memory. *ACS Appl. Mater. Interfaces* **2015**, *7*, 14288–14293.

(27) Wang, M.; Yin, Y. Magnetically Responsive Nanostructures with Tunable Optical

Properties. *J. Am. Chem. Soc.* **2016**, *138*, 6315–6323.

(28) Schauer, S.; Meier, T.; Reinhard, M.; Röhrig, M.; Schneider, M.; Heilig, M.; Kolew, A.; Worgull, M.; Hölscher, H. Tunable Diffractive Optical Elements Based on Shape-Memory Polymers Fabricated via Hot Embossing. *ACS Appl. Mater. Interfaces* **2016**, *8*, 9423–9430.

(29) Badre, C.; Marquant, L.; Alsayed, A. M.; Hough, L. A. Highly Conductive Poly (3 , 4-Ethylenedioxythiophene): Poly (Styrenesulfonate) Films Using 1-Ethyl-3-Methylimidazolium Tetracyanoborate Ionic Liquid. *Adv. Funct. Mater.* **2012**, *22*, 1–5.

(30) Liu, J.; Xie, Z.; Shang, Y.; Ren, J.; Hu, R.; Guan, B.; Wang, J.; Ikeda, T.; Jiang, L.; Wan, L.; Zhang, M.; Jiang, K.; Song, K.; Wang, J.; Badre, C.; Marquant, L.; Alsayed, A. M.; Hough, L. A. Full Color Camouflage in a Printable Photonic Blue Colored Polymer. *Adv. Funct. Mater.* **2017**, *27*, 1–5.

(31) Liu, J.; Xie, Z.; Shang, Y.; Ren, J.; Hu, R.; Guan, B.; Wang, J.; Ikeda, T.; Jiang, L. Lyophilic but Nonwettable Organosilane-Polymerized Carbon Dots Inverse Opals with Closed-Cell Structure. *ACS Appl. Mater. Interfaces* **2018**, *10*, 6701–6710.

(32) Moirangthem, M.; Engels, T.; Murphy, J.; Bastiaansen, C. W. M.; Schenning, A. P. H. J. A Photonic Shape Memory Polymer with Stable Multiple Colors. *ACS Appl. Mater. Interfaces* **2017**, *9*, 32161–32167.

(33) Moirangthem, M.; Schenning, A. P. H. J. Full Color Camouflage in a Printable Photonic Blue Colored Polymer. *ACS Appl. Mater. Interfaces* **2018**, *10*, 4168–4172.

(34) Fang, Y.; Ni, Y.; Choi, B.; Leo, S.-Y.; Gao, J.; Ge, B.; Taylor, C.; Basile, V.; Jiang, P. Chromogenic Photonic Crystals Enabled by Novel Vapor-Responsive Shape-Memory Polymers. *Adv. Mater.* **2015**, *27*, 3696–3704.

(35) Fang, Y.; Leo, S.-Y.; Ni, Y.; Yu, L.; Qi, P.; Wang, B.; Basile, V.; Taylor, C.; Jiang, P. Optically Bistable Macroporous Photonic Crystals Enabled by Thermoresponsive Shape Memory Polymers. *Adv. Opt. Mater.* **2015**, *3*, 1509–1516.

(36) Fang, Y.; Leo, S. Y.; Ni, Y.; Wang, J.; Wang, B.; Yu, L.; Dong, Z.; Dai, Y.; Basile, V.; Taylor, C.; Jiang, P. Reconfigurable Photonic Crystals Enabled by Multistimuli-Responsive Shape Memory Polymers Possessing Room Temperature Shape Processability. *ACS Appl. Mater. Interfaces* **2017**, *9*, 5457–5467.

(37) Fang, Y.; Ni, Y.; Leo, S.-Y.; Wang, B.; Basile, V.; Taylor, C.; Jiang, P. Direct Writing of Three-Dimensional Macroporous Photonic Crystals on Pressure-Responsive Shape Memory Polymers. *ACS Appl. Mater. Interfaces* **2015**, *7*, 23650–23659.

(38) Huang, W. M.; Yang, B.; An, L.; Li, C.; Chan, Y. S. Water-Driven Programmable Polyurethane Shape Memory Polymer: Demonstration and Mechanism. *Appl. Phys. Lett.* **2005**, *86*, 1–3.

(39) Lv, H.; Leng, J.; Liu, Y.; Du, S. Shape-Memory Polymer in Response to Solution. *Adv. Eng. Mater.* **2008**, *10*, 592–595.

(40) Du, H.; Zhang, J. Solvent Induced Shape Recovery of Shape Memory Polymer Based on Chemically Cross-Linked Poly(Vinyl Alcohol). *Soft Matter* **2010**, *6*, 3370–3376.

(41) Zhu, Y.; Hu, J.; Luo, H.; Young, R. J.; Deng, L.; Zhang, S.; Fan, Y.; Ye, G. Rapidly Switchable Water-Sensitive Shape-Memory Cellulose/Elastomer Nano-Composites. *Soft Matter* **2012**, *8*, 2509.

(42) Gu, X.; Mather, P. T. Water-Triggered Shape Memory of Multiblock Thermoplastic Polyurethanes (TPUs). *RSC Adv.* **2013**, *3*, 15783.

(43) Quitmann, D.; Gushterov, N.; Sadowski, G.; Katzenberg, F.; Tiller, J. C. Solvent-Sensitive

Reversible Stress-Response of Shape Memory Natural Rubber. *ACS Appl. Mater. Interfaces* **2013**, *5*, 3504–3507.

(44) Qi, X.; Yao, X.; Deng, S.; Zhou, T.; Fu, Q. Water-Induced Shape Memory Effect of Graphene Oxide Reinforced Polyvinyl Alcohol Nanocomposites. *J. Mater. Chem. A* **2014**, *2*, 2240–2249.

(45) Ramdas, M. R.; Kumar, K. S. S.; Nair, C. P. R. Heat and Solvent Responsive Polytriazole: Shape Recovery Properties in Different Solvents. *RSC Adv.* **2016**, *6*, 53602–53613.

(46) Salvekar, A. V.; Huang, W. M.; Xiao, R.; Wong, Y. S.; Venkatraman, S. S.; Tay, K. H.; Shen, Z. X. Water-Responsive Shape Recovery Induced Buckling in Biodegradable Photo-Cross-Linked Poly(Ethylene Glycol) (PEG) Hydrogel. *Acc. Chem. Res.* **2017**, *50*, 141–150.

(47) Löwenberg, C.; Balk, M.; Wischke, C.; Behl, M.; Lendlein, A. Shape-Memory Hydrogels: Evolution of Structural Principles To Enable Shape Switching of Hydrophilic Polymer Networks. *Acc. Chem. Res.* **2017**, *50*, 723–732.

(48) Sperling, L. H. *Introduction to Physical Polymer Science*; 2006; Vol. 78.

(49) Behl, M.; Lendlein, A. Shape-Memory Polymers. *Mater. Today* **2007**, *10*, 20–28.

(50) Behl, M.; Razzaq, M. Y.; Lendlein, A. Multifunctional Shape-Memory Polymers. *Adv. Mater.* **2010**, *22*, 3388–3410.

(51) Mather, P. T.; Luo, X.; Rousseau, I. A. Shape Memory Polymer Research. *Annu. Rev. Mater. Res.* **2009**, *39*, 445–471.

(52) Xie, T. Recent Advances in Polymer Shape Memory. *Polymer* **2011**, *52*, 4985–5000.

(53) Hu, J.; Zhu, Y.; Huang, H.; Lu, J. Recent Advances in Shape-Memory Polymers: Structure, Mechanism, Functionality, Modeling and Applications. *Prog. Polym. Sci.* **2012**,

37, 1720–1763.

(54) Meng, H.; Li, G. A Review of Stimuli-Responsive Shape Memory Polymer Composites. *Polym. (United Kingdom)* **2013**, *54*, 2199–2221.

(55) Zhao, Q.; Qi, H. J.; Xie, T. Recent Progress in Shape Memory Polymer: New Behavior, Enabling Materials, and Mechanistic Understanding. *Prog. Polym. Sic.*. **2014**, *49-50*, 79–120.

(56) Anthamatten, M.; Cavicchi, K.; Li, G.; Wang, A. Cold, Warm, and Hot Programming of Shape Memory Polymers. *J. Polym. Sci. Part B Polym. Phys.* **2016**, *54*, 1319–1339.

(57) Arsenault, A. C.; Clark, T. J.; Von Freymann, G.; Cademartiri, L.; Sapienza, R.; Bertolotti, J.; Vekris, E.; Wong, S.; Kitaev, V.; Manners, I.; Wang, R. Z.; John, S.; Wiersma, D.; Ozin, G. A. From Colour Fingerprinting to the Control of Photoluminescence in Elastic Photonic Crystals. *Nat. Mater.* **2006**, *5*, 179–184.

(58) Montelongo, Y.; Yetisen, A. K.; Butt, H.; Yun, S. H. Reconfigurable Optical Assembly of Nanostructures. *Nat. Commun.* **2016**, *7*, 12002.

(59) Cai, Z.; Kwak, D. H.; Punihaole, D.; Hong, Z.; Velankar, S. S.; Liu, X.; Asher, S. A. A Photonic Crystal Protein Hydrogel Sensor for Candida Albicans. *Angew. Chem. Int. Ed.* **2015**, *54*, 13036–13040.

(60) Inan, H.; Poyraz, M.; Inci, F.; Lifson, M. A.; Baday, M.; Cunningham, B. T.; Demirci, U. Photonic Crystals: Emerging Biosensors and Their Promise for Point-of-Care Applications. *Chem. Soc. Rev.* **2017**, *46*, 366–388.

(61) Chai, Z.; Hu, X.; Wang, F.; Niu, X.; Xie, J.; Gong, Q. Ultrafast All-Optical Switching. *Adv. Opt. Mater.* **2017**, *5*, 201600665.

(62) Loncar, M. Molecular Sensors: Cavities Lead the Way. *Nat. Photonics* **2007**, *1*, 565–567.

(63) Boyle, B. M.; French, T. A.; Pearson, R. M.; McCarthy, B. G.; Miyake, G. M. Structural Color for Additive Manufacturing: 3D-Printed Photonic Crystals from Block Copolymers. *ACS Nano* **2017**, *11*, 3052–3058.

(64) Song, G.; Shen, J.; Jiang, F.; Hu, R.; Li, W.; An, L.; Zou, R.; Chen, Z.; Qin, Z.; Hu, J. Hydrophilic Molybdenum Oxide Nanomaterials with Controlled Morphology and Strong Plasmonic Absorption for Photothermal Ablation of Cancer Cells. *ACS Appl. Mater. Interfaces* **2014**, *6*, 3915–3922.

(65) Shen, J.; Song, G.; An, M.; Li, X.; Wu, N.; Ruan, K.; Hu, J.; Hu, R. The Use of Hollow Mesoporous Silica Nanospheres to Encapsulate Bortezomib and Improve Efficacy for Non-Small Cell Lung Cancer Therapy. *Biomaterials* **2014**, *35*, 316–326.

(66) Fan, X.; Chung, J. Y.; Lim, Y. X.; Li, Z.; Loh, X. J. Review of Adaptive Programmable Materials and Their Bioapplications. *ACS Appl. Mater. Interfaces* **2016**, *8*, 33351–33370.

(67) Chan, B. Q. Y.; Low, Z. W. K.; Heng, S. J. W.; Chan, S. Y.; Owh, C.; Loh, X. J. Recent Advances in Shape Memory Soft Materials for Biomedical Applications. *ACS Appl. Mater. Interfaces* **2016**, *8*, 10070–10087.

(68) Jiang, P.; Bertone, J. F.; Hwang, K. S.; Colvin, V. L. Single-Crystal Colloidal Multilayers of Controlled Thickness. *Chem. Mater.* **1999**, *11*, 2132–2140.

(69) Asif, S. A. S.; Wahl, K. J.; Colton, R. J. Nanoindentation and Contact Stiffness Measurement Using Force Modulation with a Capacitive Load-Displacement Transducer. *Rev. Sci. Instrum.* **1999**, *70*, 2408–2413.

(70) Johnson, K. L.; Kendall, K.; Roberts, A. D. Surface Energy and the Contact of Elastic Solids. *Proc. R. Soc. A Math. Phys. Eng. Sci.* **1971**, *324*, 301–313.

(71) Velev, O. D.; Gupta, S. Materials Fabricated by Micro- and Nanoparticle Assembly - The

Challenging Path from Science to Engineering. *Adv. Mater.* **2009**, *21*, 1897–1905.

(72) Ulman, A. *An Introduction to Ultrathin Organic Films: From Langmuir-Blodgett to Self-Assembly*; 2013.

(73) Salvekar, A. V.; Huang, W. M.; Xiao, R.; Wong, Y. S.; Venkatraman, S. S.; Tay, K. H.; Shen, Z. X. Water-Responsive Shape Recovery Induced Buckling in Biodegradable Photo-Cross-Linked Poly(Ethylene Glycol) (PEG) Hydrogel. *Acc. Chem. Res.* **2017**, *50*, 141–150.

(74) Löwenberg, C.; Balk, M.; Wischke, C.; Behl, M.; Lendlein, A. Shape-Memory Hydrogels: Evolution of Structural Principles To Enable Shape Switching of Hydrophilic Polymer Networks. *Acc. Chem. Res.* **2017**, *50*, 723–732.

(75) Zhang, C.; Cano, G. G.; Braun, P. V. Linear and Fast Hydrogel Glucose Sensor Materials Enabled by Volume Resetting Agents. *Adv. Mater.* **2014**, *26*, 5678–5683.

(76) Zhang, C.; Losego, M. D.; Braun, P. V. Hydrogel-Based Glucose Sensors: Effects of Phenylboronic Acid Chemical Structure on Response. *Chem. Mater.* **2013**, *25*, 3239–3250.

(77) Hirotsu, S. Softening of Bulk Modulus and Negative Poisson's Ratio near the Volume Phase Transition of Polymer Gels. *J. Chem. Phys.* **1991**, *94*, 3949–3957.

(78) Shibayama, M.; Tanaka, T. Volume Phase Transition and Related Phenomena of Polymer Gels. *Adv. Polym. Sci.* **1993**, *109*, 1–62.

(79) Mancarella, F.; Style, R. W.; Wettlaufer, J. S. Interfacial Tension and a Three-Phase Generalized Self-Consistent Theory of Non-Dilute Soft Composite Solids. *Soft Matter* **2016**, *12*, 2744–2750.

(80) Cai, Z.; Luck, L. A.; Punihaole, D.; Madura, J. D.; Asher, S. A. Photonic Crystal Protein

Hydrogel Sensor Materials Enabled by Conformationally Induced Volume Phase Transition. *Chem. Sci.* **2016**, *49*, 1993–2007.

Table of Contents Graphic